SOLUS | SMART OPTICAL AND ULTRASOUND DIAGNOSTICS OF BREAST CANCER

Project title: Smart Optical and Ultrasound Diagnostics of Breast Cancer

Grant Agreement: 731877

Call identifier: H2020-ICT-2016-1

Topic: ICT-29-2016 Photonics KET 2016

Deliverable 4.7: Performance assessment of DOT with US priors

Leader partner:	Beneficiary 5, UCL
Author(s):	Simon Arridge (UCL), Giuseppe Di Sciacca (UCL), Laura Di Sieno (POLIMI), Giulia Maffeis (POLIMI), Andrea Farina (POLIMI), Alberto Dalla Mora (POLIMI), Antonio Pifferi (POLIMI), Paola Taroni (POLIMI)
Work Package:	4
Estimated delivery:	Month 36
Actual delivery:	Month 56
Type:	Report
Dissemination level:	Public

Tables of contents

Abbreviations

Acc.	Accuracy error
Broad.	Broadening
C	Contrast
CNR	Contrast-to-Noise ratio
Disp.	Displacement
DOT	Diffuse Optical Tomography
PV1	Perturbation Volume 1
PV2	Perturbation Volume 2
FOM	Figure of Merit
Tk0	Zeroth order Tikhonov regularisation
US	Ultrasound
US-Tk1	US-weighted first order Tikhonov regularisation

1. Introduction

The aim of this deliverable is to assess the performances of DOT with US priors with the tools and strategies identified by D2.2 and D2.3. Results have been obtained from tests on a set of multimodal phantoms, described in D4.4. A series of quantitatively interesting figures of merit were extracted as foreseen by D4.2.

In Section 2, we give an overview of the data analysed and the prior extraction procedure. In Section 3 we show the results and give some quantitative indications.

2. Overview of Data

A total of 6 heterogeneous acquisitions (considering only the first-delay of the time-gated acquisitions, i.e., a measurement where the whole curve has been recorded) were taken with the SOLUS probe.

All phantoms in D4.4 consisted of a cylindrical inclusion in an otherwise homogeneous medium. Inclusions can have volume of either 1 cm^3 or 6 cm^3. In this deliverable, we focus only on the bigger inclusion (6 cm^3).

For each bulk, a homogeneous measurement (i.e., with the inclusion made of the same material – Ecoflex - and with the same optical properties) was taken as reference. After that, Ecoflex inclusions were replaced with Sylgard ones, of different optical properties with respect to the bulk and the probe was aligned to have the inclusion at the centre of the operative region of the SOLUS probe. In this position, a heterogenous measurement was taken.

The operation was repeated for each of the three bulks available, each time with a different optical absorption coefficient of the inclusion. Only a contrast in absorption was selected for this study.

An overview of the optical measurements is displayed in Table 2.1.

Table 2.1 Set of the measurements analysed for the assessment of US priors on phantoms. Each heterogeneous measurement is categorised as a Phantom, for a total of 6 phantoms.

Bulk properties μ'_s, μ_a	Inclusion properties μ'_s, μ_a	Type Of Measure μ'_s, μ_a
1 mm^{-1}, 0.005 mm^{-1}	1 mm^{-1}, 0.005 mm^{-1}	Homogeneous
1 mm^{-1}, 0.005 mm^{-1}	1 mm^{-1}, 0.01 mm^{-1}	Heterogeneous | PHANTOM 1
1 mm^{-1}, 0.005 mm^{-1}	1 mm^{-1}, 0.02 mm^{-1}	Heterogeneous | PHANTOM 2
1 mm^{-1}, 0.01 mm^{-1}	1 mm^{-1}, 0.01 mm^{-1}	Homogeneous
1 mm^{-1}, 0.01 mm^{-1}	1 mm^{-1}, 0.005 mm^{-1}	Heterogeneous | PHANTOM 3
1 mm^{-1}, 0.01 mm^{-1}	1 mm^{-1}, 0.02 mm^{-1}	Heterogeneous | PHANTOM 4
1 mm^{-1}, 0.02 mm^{-1}	1 mm^{-1}, 0.02 mm^{-1}	Homogeneous
1 mm^{-1}, 0.02 mm^{-1}	1 mm^{-1}, 0.01 mm^{-1}	Heterogeneous | PHANTOM 5
1 mm^{-1}, 0.02 mm^{-1}	1 mm^{-1}, 0.04 mm^{-1}	Heterogeneous | PHANTOM 6

The inclusion is a cylinder of volume 6 cm^3 with height 15 mm and radius 11 mm, whose top is set at a depth of 15 mm (in agreement with one of the paradigmatic scenarios defined in D2.1). The experimental conditions allowed to consider the same US image for each of the measured phantoms.

The image has been segmented via the method presented in D2.2, via a manual segmentation of the US B-mode image and a 3D extraction based on the distance transform of the resulting binary image (we refer to [Di Sciacca G et al. 2021 "Enhanced diffuse optical tomographic reconstruction using concurrent ultrasound information" Phil. Trans. R. Soc. A 379: 20200195. https://doi.org/10.1098/rsta.2020.0195] for details). The result of the prior extraction from the US B-mode image (reported in Figure 2.1) is shown in Figure 2.2 with a comparison with the ground truth.

For reference in the following, the x-axis is the direction of maximum elongation of the US transducer, z is the depth of the phantom so that an US image is taken on the x-z plane. The y axis is the orthogonal to x and z. The origin is set on the surface of the phantom, in the geometrical centre of the transducer.

With respect to the ground truth, the centre of the extrapolated inclusion resulted being displaced by -0.35, 0 and 1.1 mm respectively along x, y and z. The difference in maximum elongation with respect to the ground truth resulted respectively as 0, 4 and 2 mm.

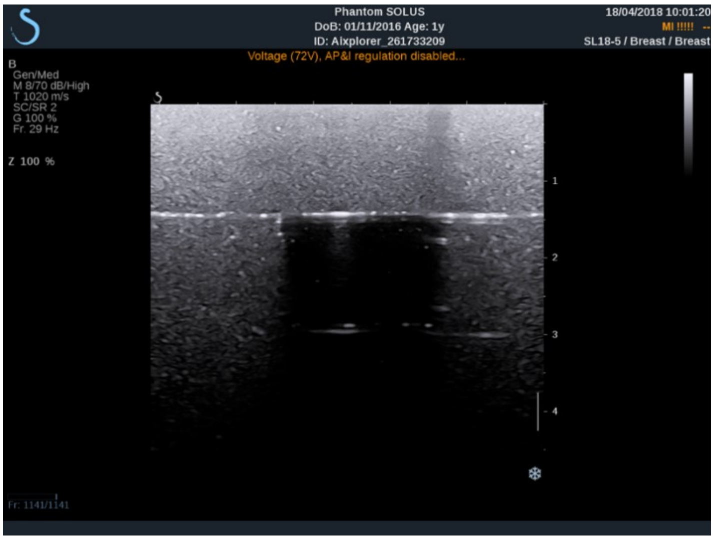

Figure 2.1 Ultrasound B-mode image of inclusion as from D4.4.

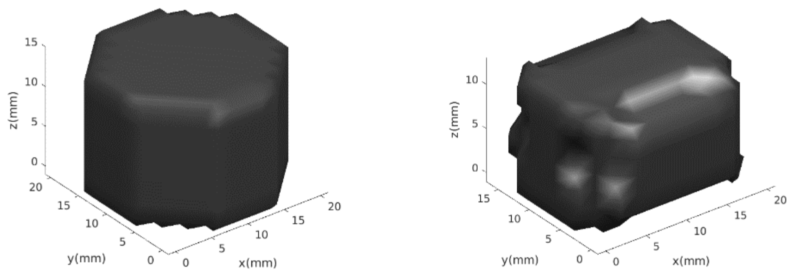

Figure 2.2 Left: Cylindrical Inclusion as would appear in the computational grid. Right: Prior as extracted from the US image

3. Results

The strategy chosen for reconstruction was the 1.b as described in Deliverable D2.3. For each wavelength a separate reconstruction of reduced scattering and absorption is employed. Once the optical properties of the bulk $\mu_{a,0}$, $\mu'_{s,0}$ are estimated from the reference measurement with a nonlinear fit, the Jacobian J of the diffusive model around $\mu_{a,0}$, $\mu'_{s,0}$ is calculated. The information contained in the US image is exploited as a soft prior, via a US dependent penalty term R_{US} . So that, for each wavelength:

$$[\tilde{\mu}_a, \tilde{\mu}_s] = [\mu_{a,0}, \mu'_{s,0}] + argmin \quad ||S\,J\,[\Delta\mu_a, \Delta\mu'_s] - \Delta M||^2 + \tau\, R_{US}\,[\Delta\mu_{a,0}, \Delta\, \mu''_{s,0}],$$

where $[\tilde{\mu}_a, \tilde{\mu}_s]$ is the final reconstruction, ΔM is the difference between the heterogenous and homogenous measurements, S is diagonal matrix of the inverse standard deviations of each measurement and τ is a regularisation parameter.

The optical reconstruction for each phantom took approximately 10 minutes, with the Jacobian calculation employing circa 20 s per wavelength. The optimal regularisation parameter for each reconstruction with *a priori* information oscillates between 0.2 and 1. Each reconstruction is shown as a set of one tomographic image per wavelength. Each tomographic image is shown as slices representing different depths from left to right, from top to bottom. The top-left slice represents the part of the volume close to the top surface of the phantom. We show results in the case of Tikhonov 0 regularisation (Tk0) and US prior edge-weighted Tikhonov 1 (US-Tk1) regularisation.

Each reconstruction is quantified by a set of figures of merit (FOMs): contrast (C), contrast-to-noise ratio (CNR), accuracy error (Acc.), displacement (Disp.) and broadening (Broad.). All of these FOMs depend on the region where the inclusion is supposed to be. When no prior information on morphology is available, the portion of domain occupied by the inclusion is retrieved by considerations on the contrast and standard deviation of the tomographic images. In the following, we refer to this procedure as PV1. When a US prior is present, also quantification based on this information can be performed; we refer to this as PV2.

With respect to D4.2, the definition of C and CNR has been changed. In D4.2 these FOMs were defined as:

$$C = \frac{N_P - N_0}{N_0}; \qquad CNR = \frac{N_P - N_0}{\sigma(N_0)},$$

where N_0 and N_P are the number of photon counts evaluated inside a given temporal window chosen along the histogram of the photons time of flight in the homogeneous and heterogeneous case respectively and $\sigma(N_0)$ is the standard deviation of N_0 due to the Poisson statistics and other effects (*e.g.,* laser power fluctuations). However, this definition was derived by an existing protocol (i.e., NEUROPT protocol, see [H. Wabnitz et al., "Performance assessment of time- domain optical brain imagers, part 2: nEUROPt protocol," Journal of Biomedical Optics 19(8), 086012, 2014]) devised for the performance assessment of non-tomographic systems (*i.e.*, with few source-detector pairs). In our case here, for a single tomographic image at a single wavelength, this definition resulted to generate a number of different values of C and CNR depending on the source-detector pair considered (*i.e.*, 64 possible cases), the delay at which the detector is time-gated (*i.e.*, many possible cases) and the position of the temporal window used for analysis chosen along the histogram of the photons time of flight (*i.e.*, many possible cases). Furthermore, the previous definition required to combine in each single FOM measurables referred to the homogeneous and heterogeneous acquisitions, which are implemented using phantoms with different inclusions (*i.e.*, Ecoflex and Sylgard). Therefore, after evaluating these first SOLUS experimental results, a better definition was introduced to provide unambiguous and univocal FOMs, more linked to tomographic measurables and that can be computed from a single tomographic measurement at each wavelength:

$$C = \frac{\tilde{\mu}_{a,s}^{Pert} - \tilde{\mu}_{a,s}^{Bulk}}{\tilde{\mu}_{a,s}^{Bulk}}; \qquad CNR = \frac{\tilde{\mu}_{a,s}^{Pert} - \tilde{\mu}_{a,s}^{Bulk}}{\sigma\left(\tilde{\mu}_{a,s}^{Bulk}\right)},$$

where $\tilde{\mu}_{a,s}^{Pert}$ and $\tilde{\mu}_{a,s}^{Bulk}$ are the reconstructed absorption (*a*) or reduced scattering (*s*) coefficients inside (*Pert*) or outside (*Bulk*) the perturbation volume, while $\sigma\left(\tilde{\mu}_{a,s}^{Bulk}\right)$ is the standard deviation of the reconstructed optical properties in the bulk volume.

As an additional advantage of this definition, the targeted C can be defined simply by replacing the reconstructed optical properties with the reference ones taken from the phantom kit characterization, providing in this way a term of comparison to evaluate experimental values.

There is no unique way to calculate the Perturbation volume. One choice (PV1) is as follows: for each wavelength and generical reconstructed optical property $\tilde{\mu}(x, y, z)$, assume it to be the region for which the values of the reconstructions are bigger that a factor 4 of its fluctuations. So that:

$$Pert = (x, y, z) \quad \text{s.t.} \quad \frac{\tilde{\mu} - \text{median}\,\tilde{\mu}}{\sigma(\tilde{\mu})} > 4.$$

Otherwise, when a US prior is present, *Pert* can be assumed to coincide with the prior itself (PV2). This choice only depends on the morphological information used in reconstruction and is independent from the fluctuations in the reconstructions thus giving a more accurate quantification of the lesion's properties.

The other FOMs have been computed in agreement with definitions provided in D4.2.

PHANTOM 1: Bulk of μ_a = 0.005 mm^{-1} with Inclusion of μ_a = 0.01 mm^{-1}

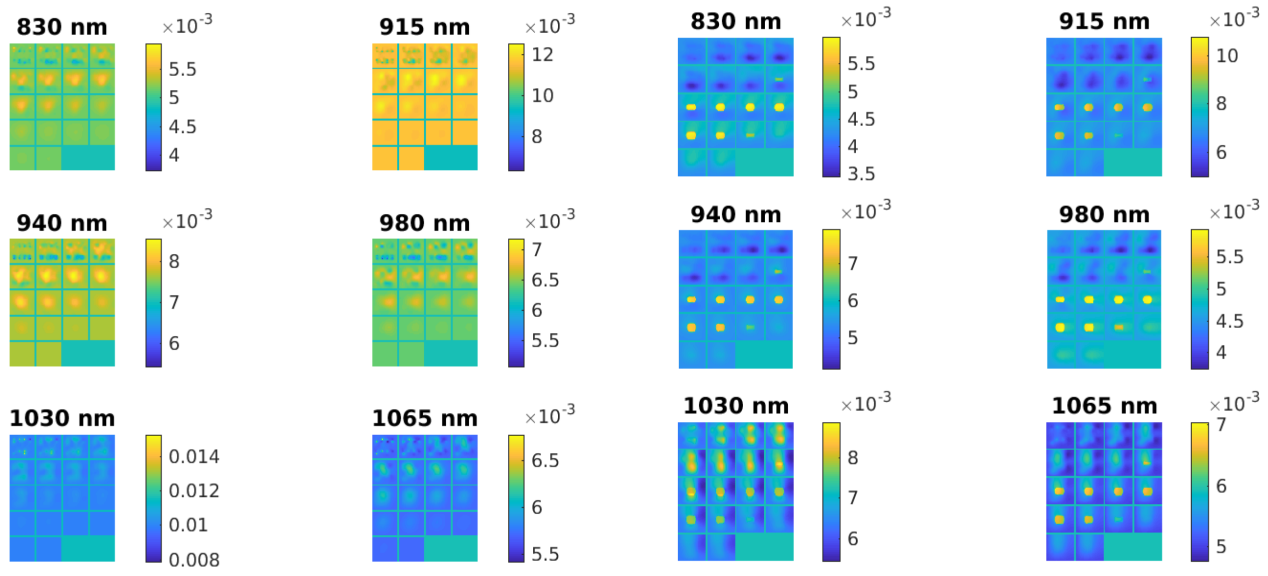

Figure 3.1 Left: Reconstruction of absorption for Phantom 1 when Tk0 regularisation with parameter of 0.1 is applied. Right: Reconstruction of absorption for Phantom 1 when US-Tk1 regularisation with parameter of 0.2 is applied.

Reconstruction for the phantom with bulk of μ_{a0} = 0.005 mm^{-1} and inclusion of μ_{a0} = 0.01 mm^{-1} is shown in Figure 3.1. We note that the reconstructions for the wavelengths 635 nm and 670 nm are missing due to a recurring probe error during the measurements for this configuration. All tables from Table 3.1 to Table 3.5 (each one displaying at all available wavelengths the figures of merit listed above) show a clear advantage in the use of a US prior, especially when using PV2 for quantification. Contrast is enhanced using a US prior. Accuracy on the absorption of the inclusion shows an error contained to ca 10% for most wavelengths. Results on the geometry show that PV1 is a source of errors for the domain geometry retrieval. This is due to the large rate of spatial variations in the tomographic images and it holds true for all the reconstructions here presented.

Table 3.1 Table displaying the target and reconstructed Contrast for Phantom 1 at each wavelength.

C	830 nm	915 nm	940 nm	980 nm	1030 nm	1065 nm
Target	1.5	0.34	1.41	1.25	0.9	1.37
Tk0; PV1	0.03	-0.02	0.02	0.01	0.08	0.04
US-Tk1; PV1	0.15	0.06	0.14	0.07	0.14	0.16
US-Tk1; PV2	0.32	0.36	0.34	0.25	0.16	0.21

Table 3.2 Table displaying the Contrast-to-Noise Ratio for Phantom 1 at each wavelength. Sign of Target is positive.

CNR	830 nm	915 nm	940 nm	980 nm	1030 nm	1065 nm
Tk0; PV1	3.4	-1.92	2.26	1.71	6.36	5.1
US-Tk1; PV1	2.84	1.26	4.23	2.1	2.2	3.94
US-Tk1; PV2	5.32	5.6	7.52	5.87	1.87	3.9

Table 3.3 Table displaying the Accuracy Error for Phantom 1 at each wavelength.

Acc.	830 nm	915 nm	940 nm	980 nm	1030 nm	1065 nm
Tk0; PV1	-0.43	0.25	0	-0.47	0.39	-0.18
US-Tk1; PV1	-0.47	-0.22	-0.22	-0.6	-0.04	-0.17
US-Tk1; PV2	-0.4	-0	-0.09	-0.54	-0.01	-0.12

Table 3.4 Table displaying the Displacement of the retrieved inclusion for Phantom 1 at each wavelength. The Euclidean distance between the centre of the target and reconstruction in mm is given.

Displ.(mm)	830 nm	915 nm	940 nm	980 nm	1030 nm	1065 nm
Tk0; PV1	11.36	13.85	11.64	13.41	13.81	12.64
US-Tk1; PV1	5.02	8.96	8.2	9.38	9.94	11.1
US-Tk1; PV2	1.15	1.15	1.15	1.15	1.15	1.15

Table 3.5 Table displaying the Broadening of the retrieved inclusion for Phantom 1 at each wavelength. The average difference between the maximum elongation along the three dimensions of target and reconstruction in mm is given.

Broad. (mm)	830 nm	915 nm	940 nm	980 nm	1030 nm	1065 nm
Tk0; PV1	14.67	13.33	13.33	13.33	15.33	12
US-Tk1; PV1	2.67	10.67	6	6	15.33	10
US-Tk1; PV2	-2	-2	-2	-2	-2	-2

PHANTOM 2: Bulk of μ_a= 0.005 mm^{-1} with Inclusion of μ_a= 0.02 mm^{-1}

Reconstruction for the Phantom 2, of bulk of μ_{a0} = 0.005 mm^{-1} and inclusion of μ_{a0} = 0.02 mm^{-1} is shown in Figure 3.2. We note, as in the previous subsection, that the reconstructions for the wavelengths 635 nm and 670 nm are missing due to a recurring probe error during the measurements for this configuration. The quality of the reconstructions results to be visually noisier than Figure 3.1. This reflects in the figures of merit displayed from Table 3.6 to Table 3.10 and, in particular, by the CNR (see Table 3.7) which presents an appreciably large values only at 830 nm and 980 nm. The poor quality of the reconstruction for this phantom might be due to experimental anomalies.

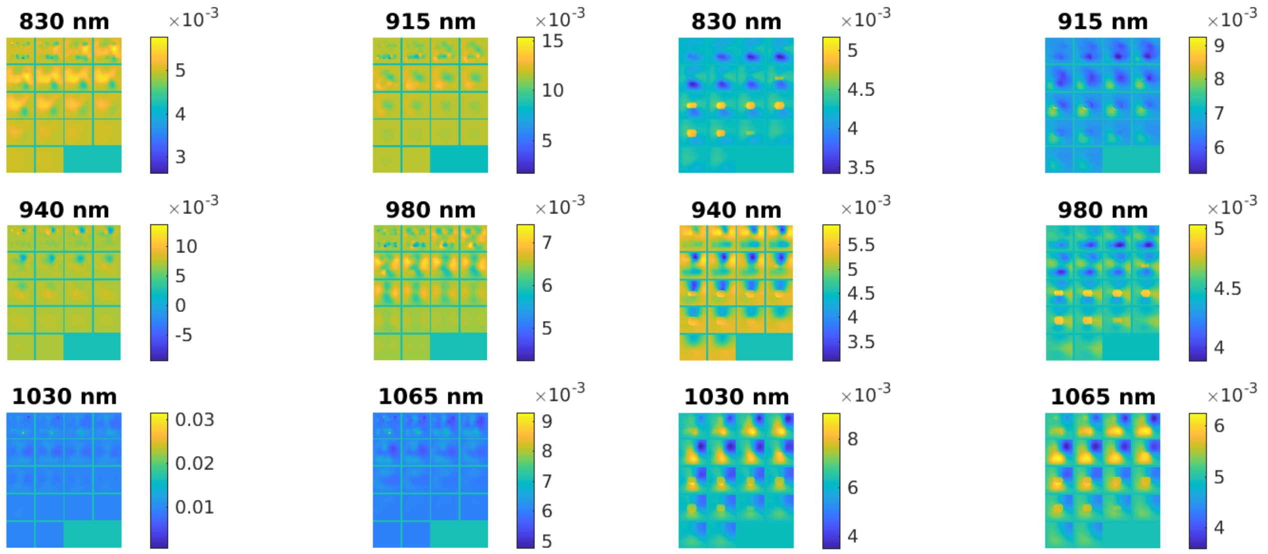

Figure 3.2 Left: Reconstruction of absorption for Phantom 2 when Tk0 regularisation with parameter of 0.05 is applied. Right: Reconstruction of absorption for Phantom 2 when US-Tk1 regularisation with parameter of 0.2 is applied.

Table 3.6 Table displaying the target and reconstructed Contrast for Phantom 2 at each wavelength.

C	830 nm	915 nm	940 nm	980 nm	1030 nm	1065 nm
Target	4.09	1.32	4.06	3.98	2.6	3.86
Tk0; PV1	0.02	-0.01	-0.3	0.01	0.01	0.02
US-Tk1; PV1	-0.02	0.03	-0.19	-0.02	-0.1	-0.08
US-Tk1; PV2	0.14	-0.03	0.04	0.08	0.15	0.1

Table 3.7 Table displaying the Contrast-to-Noise Ratio for Phantom 2 at each wavelength. Sign of Target is positive.

CNR	830 nm	915 nm	940 nm	980 nm	1030 nm	1065 nm
Tk0; PV1	1.3	-0.39	-7.01	0.47	0.2	1.2
US-Tk1; PV1	-0.75	0.69	-4.3	-1.2	-1.21	-1.41
US-Tk1; PV2	4.06	-0.46	0.47	2.92	1.06	1.07

Table 3.8 Table displaying the Accuracy Error for Phantom 2 at each wavelength.

Acc.	830 nm	915 nm	940 nm	980 nm	1030 nm	1065 nm
Tk0; PV1	-0.73	-0.36	-0.68	-0.69	-0.39	-0.62
US-Tk1; PV1	-0.78	-0.62	-0.74	-0.79	-0.65	-0.71
US-Tk1; PV2	-0.74	-0.64	-0.67	-0.77	-0.56	-0.66

Table 3.9 Table displaying the Displacement of the retrieved inclusion for Phantom 2 at each wavelength. The Euclidean distance between the centre of the target and reconstruction in mm is given.

Displ. (mm)	830 nm	915 nm	940 nm	980 nm	1030 nm	1065 nm
Tk0; PV1	10.71	15.03	18.8	10.64	14.75	13.58
US-Tk1; PV1	12.74	12.45	16.26	10.22	17.61	17.34
US-Tk1; PV2	1.15	1.15	1.15	1.15	1.15	1.15

Table 3.10 Table displaying the Broadening of the retrieved inclusion for Phantom 2 at each wavelength. The average difference between the maximum elongation along the three dimensions of target and reconstruction in mm is given.

Broad. (mm)	830 nm	915 nm	940 nm	980 nm	1030 nm	1065 nm
Tk0; PV1	18	17.33	8.67	15.33	13.33	12.67
US-Tk1; PV1	9.33	14	12	15.33	10	11.33
US-Tk1; PV2	-2	-2	-2	-2	-2	-2

PHANTOM 3: Bulk of μ_a = 0.01 mm^{-1} with Inclusion of μ_a = 0.005 mm^{-1}

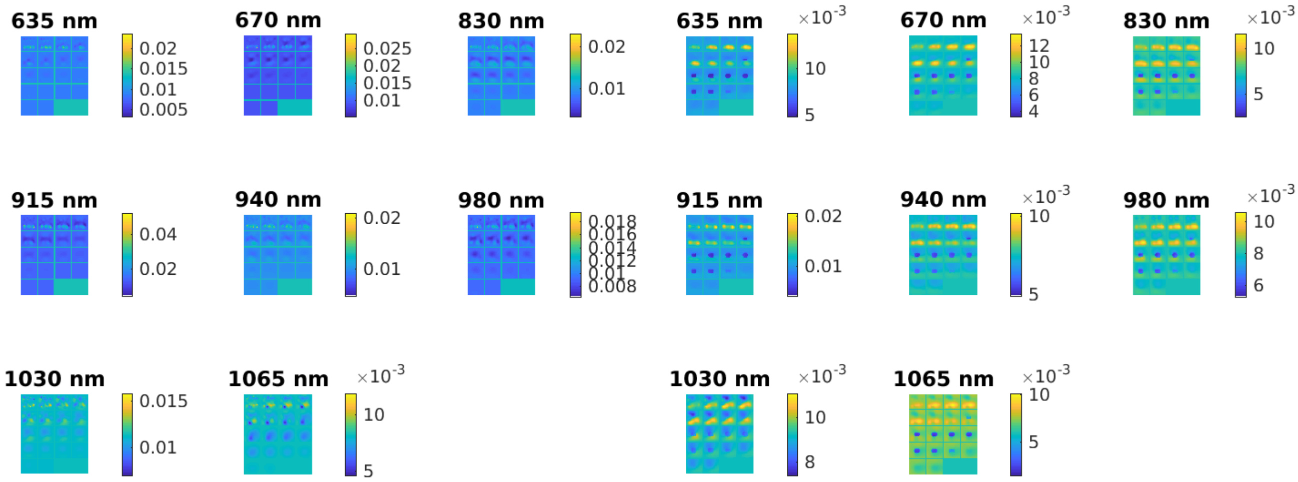

Figure 3.3 Left: Reconstruction of absorption for Phantom 3 when Tk0 regularisation with parameter of 0.05 is applied. Right: Reconstruction of absorption for Phantom 3 when US-Tk1 regularisation with parameter of 0.2 is applied.

Reconstruction for the phantom with bulk of μ_a = 0.01 mm^{-1} and inclusion of μ_a = 0.005 mm^{-1} is shown in Figure 3.3**Error! Reference source not found.**. The figures of merit are shown from Table 3.11 to Table 3.15 and, as for Phantom 1, depict generally better results when using US priors. Table 3.11 and Table 3.12 show the reconstructed contrast and the CNR highlighting how the difference between values of inclusion and bulk is at least 2 times larger than the std of the fluctuations in the bulk. Accuracy for PV2 and US prior is shown to be contained for most wavelengths at 20%.

Table 3.11 Table displaying the target and reconstructed Contrast for Phantom 3 at each wavelength.

C	635 nm	670 nm	830 nm	915 nm	940 nm	980 nm	1030 nm	1065 nm
Target	-0.42	-0.41	-0.5	-0.3	-0.52	-0.54	-0.42	-0.5
Tk0; PV1	0.14	0.11	0.06	0.05	0.05	-0.02	-0	-0.09
US-Tk1; PV1	0.15	0.12	0.06	0.21	0.07	0.06	0.01	-0.18
US-Tk1; PV2	-0.31	-0.38	-0.47	-0.41	-0.2	-0.23	-0.08	-0.58

Table 3.12 Table displaying the Contrast-to-Noise Ratio for Phantom 3 at each wavelength. Sign of Target is negative.

CNR	635 nm	670 nm	830 nm	915 nm	940 nm	980 nm	1030 nm	1065 nm
Tk0; PV1	5.07	3.09	0.97	0.87	1.44	-0.46	-0.2	-2.49
US-Tk1; PV1	2.63	2	0.79	2.52	1.29	1.32	0.2	-2.77
US-Tk1; PV2	-2.83	-3.42	-4.33	-2.8	-2.72	-3.51	-1.5	-6.72

Table 3.13 Table displaying the Accuracy Error for Phantom 3 at each wavelength.

Acc.	635 nm	670 nm	830 nm	915 nm	940 nm	980 nm	1030 nm	1065 nm
Tk0; PV1	0.85	1.05	1.41	0.8	1.87	1.74	1.08	0.91
US-Tk1; PV1	0.76	0.92	1.17	0.49	1.25	1.57	0.74	0.54
US-Tk1; PV2	0.08	0.08	0.11	-0.25	0.7	0.9	0.59	-0.2

Table 3.14 Table displaying the Displacement of the retrieved inclusion for Phantom 3 at each wavelength. The Euclidean distance between the centre of the target and reconstruction in mm is given.

Displ.(mm)	635 nm	670 nm	830 nm	915 nm	940 nm	980 nm	1030 nm	1065 nm
Tk0; PV1	18.09	16.52	13.67	16.59	15.28	13.44	11.82	12.16
US-Tk1; PV1	15.18	14.3	13.76	15.88	14.99	14.41	10.46	9.54
US-Tk1; PV2	1.15	1.15	1.15	1.15	1.15	1.15	1.15	1.15

Table 3.15 Table displaying the Broadening of the retrieved inclusion for Phantom 3 at each wavelength. The average difference between the maximum elongation along the three dimensions of target and reconstruction in mm is given.

Broad.(mm)	635 nm	670 nm	830 nm	915 nm	940 nm	980 nm	1030 nm	1065 nm
Tk0; PV1	6.67	13.33	12.67	10	12.67	10.67	14	12
US-Tk1; PV1	12	12.67	13.33	10.67	10	13.33	15.33	8
US-Tk1; PV2	-2	-2	-2	-2	-2	-2	-2	-2

PHANTOM 4: Bulk of μ_a = 0.01mm^{-1} with Inclusion of μ_a = 0.02 mm^{-1}

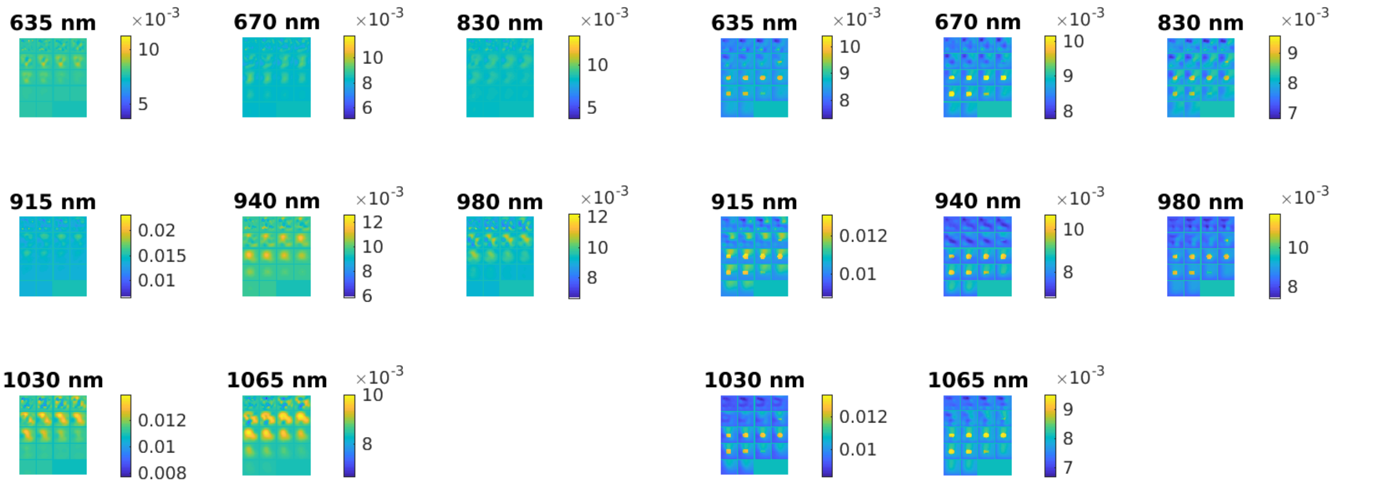

Figure 3.4 Left: Reconstruction of absorption for Phantom 4 when Tk0 regularisation with parameter of 0.05 is applied. Right: Reconstruction of absorption for Phantom 4 when US-Tk1 regularisation with parameter of 0.2 is applied.

Reconstruction for the phantom with bulk of μ_a = 0.01 mm^{-1} and inclusion of μ_a = 0.02 mm^{-1} is shown in Figure 3.4. In this case too, the reconstructions with US *a priori* information show images of improved quality, where the inclusion is more easily detected. A quantification of the quality of the reconstruction is shown from Table 3.16 to Table 3.20. Also in this case the contrast is improved by the use of US priors, but the sign is correctly reconstructed for all the reconstruction strategies here presented. The accuracy error shows an underestimation of the absorption coefficient of the inclusion of ca ~50%.

Table 3.16 Table displaying the target and reconstructed contrast for Phantom 4 at each wavelength.

C	635 nm	670 nm	830 nm	915 nm	940 nm	980 nm	1030 nm	1065 nm
Target	1.07	1.19	1.14	0.86	1.21	1.21	0.98	1.2
Tk0; PV1	0.07	0.06	0.04	0.07	0.07	0.07	0.08	0.08
US-Tk1; PV1	0.06	0.1	0.02	0.13	0.16	0.14	0.17	0.11
US-Tk1; PV2	0.14	0.15	0.11	0.17	0.25	0.23	0.25	0.19

Table 3.17 Table displaying the Contrast-to-Noise ratio for Phantom 4 at each wavelength. Sign of target is positive.

CNR	635 nm	670 nm	830 nm	915 nm	940 nm	980 nm	1030 nm	1065 nm
Tk0; PV1	4.06	3.38	2.71	3.87	3.35	2.76	3.22	3.2
US-Tk1; PV1	2.86	4.28	0.62	3.37	3.54	3.94	3.96	3.33
US-Tk1; PV2	5.35	6.02	3.12	3.25	4.58	5.75	4.66	5.25

Table 3.18 Table displaying the Accuracy Error for Phantom 4 at each wavelength.

Acc.	635 nm	670 nm	830 nm	915 nm	940 nm	980 nm	1030 nm	1065 nm
Tk0; PV1	-0.56	-0.52	-0.45	-0.31	-0.35	-0.39	-0.33	-0.45
US-Tk1; PV1	-0.53	-0.48	-0.5	-0.46	-0.43	-0.39	-0.38	-0.5
US-Tk1; PV2	-0.49	-0.45	-0.45	-0.42	-0.38	-0.34	-0.33	-0.46

Table 3.19 Table displaying the Displacement of the retrieved inclusion for Phantom 4 at each wavelength. The Euclidean distance between the centre of the target and reconstruction in mm is given.

Displ.(mm)	635 nm	670 nm	830 nm	915 nm	940 nm	980 nm	1030 nm	1065 nm
Tk0; PV1	10.92	9.03	10.6	14.29	9.46	10.85	11.61	9.37
US-Tk1; PV1	9.18	6.12	12.31	16.28	11.14	5.22	13.08	8.78
US-Tk1; PV2	1.15	1.15	1.15	1.15	1.15	1.15	1.15	1.15

Table 3.20 Table displaying the Broadening of the retrieved inclusion for Phantom 4 at each wavelength. The average difference between the maximum elongation along the three dimensions of target and reconstruction in mm is given.

Broad.(mm)	635 nm	670 nm	830 nm	915 nm	940 nm	980 nm	1030 nm	1065 nm
Tk0; PV1	19.33	15.33	17.33	16.67	12	12	12.67	14.67
US-Tk1; PV1	2.67	0.67	5.33	17.33	10	4	10.67	8
US-Tk1; PV2	-2	-2	-2	-2	-2	-2	-2	-2

PHANTOM 5: Bulk of μ_a = 0.02 mm^{-1} with Inclusion of μ_a = 0.01 mm^{-1}

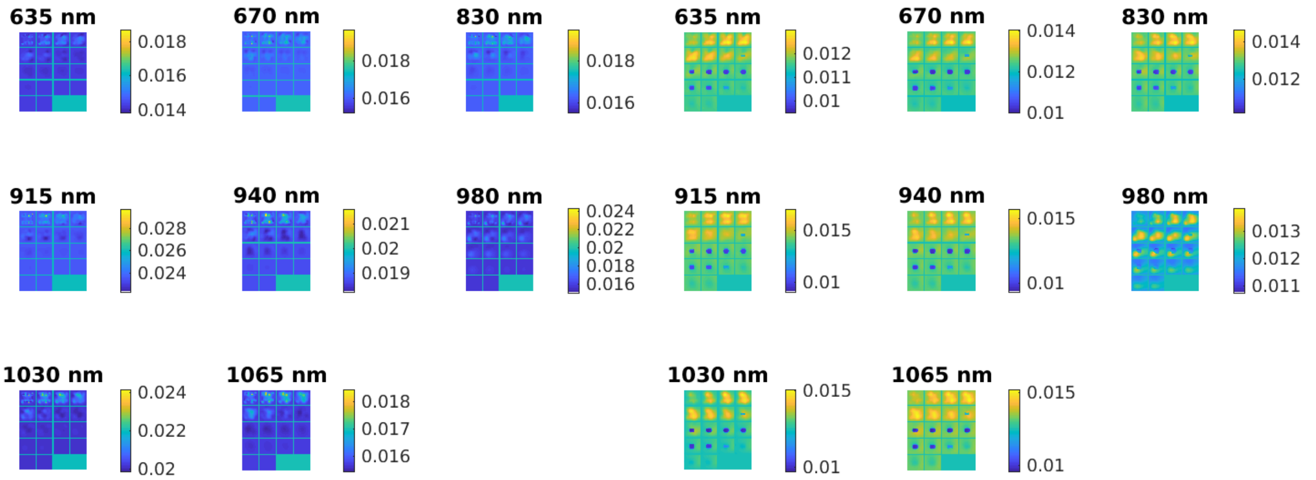

Figure 0.1 Left: Reconstruction of absorption for Phantom 5 when Tk0 regularisation with parameter of 0.2 is applied. Right: Reconstruction of absorption for Phantom 5 when US-Tk1 regularisation with parameter of 0.5 is applied.

Reconstruction for the phantom with bulk of μ_a = 0.02 mm^{-1} and inclusion of μ_a = 0.01 mm^{-1} is shown in **Error! Reference source not found.**. From a visual overview of the tomographic image, US priors can be seen to be useful for cleaner images for all cases apart from at 980 nm. The poor quality of the reconstructions at 980 nm can also be seen by the quantifications, that are displayed from Table 0.1 to Table 0.5. Also, in this case, the use of an *a priori* information improves the quantification of all figures. In particular, the contrast is reconstructed with the correct sign, even though underestimated with respect to the target. The accuracy error results to be contained to ~30% for most of the wavelengths.

Table 0.1 Table displaying the target and reconstructed contrast for Phantom 5 at each wavelength.

C	635 nm	670 nm	830 nm	915 nm	940 nm	980 nm	1030 nm	1065 nm
Target	-0.47	-0.45	-0.49	-0.36	-0.48	-0.51	-0.42	-0.46
Tk0; PV1	0.04	0.03	0.04	0.03	0.03	0.07	0.05	0.05
US-Tk1; PV1	0	-0.02	-0.01	-0.02	-0.04	0.08	0.02	-0.03
US-Tk1; PV2	-0.14	-0.16	-0.16	-0.27	-0.24	-0.03	-0.19	-0.24

Table 0.2 Table displaying the Contrast-to-Noise Ratio for Phantom 5 at each wavelength. Sign of target is negative.

CNR	635 nm	670 nm	830 nm	915 nm	940 nm	980 nm	1030 nm	1065 nm
Tk0; PV1	8.66	7.95	7.98	6.72	6.39	5.92	9.66	8.82
US-Tk1; PV1	0.26	-1.13	-0.41	-0.75	-1.79	2.93	0.62	-1.24
US-Tk1; PV2	-5.53	-6.23	-5.89	-6.14	-6.87	-0.82	-4.76	-6.41

Table 0.3 Table displaying the Accuracy Error for Phantom 5 at each wavelength.

Acc.	635 nm	670 nm	830 nm	915 nm	940 nm	980 nm	1030 nm	1065 nm
Tk0; PV1	0.57	0.82	1.15	0.96	1.49	1.32	1.21	1.02
US-Tk1; PV1	0.25	0.34	0.65	0.12	0.67	0.8	0.36	0.58
US-Tk1; PV2	0.07	0.16	0.41	-0.15	0.33	0.62	0.09	0.26

Table 0.4 Table displaying the Displacement of the retrieved inclusion for Phantom 5 at each wavelength. The Euclidean distance between the centre of the target and reconstruction in mm is given.

Displ.(mm)	635 nm	670 nm	830 nm	915 nm	940 nm	980 nm	1030 nm	1065 nm
Tk0; PV1	17.01	16.52	16.77	16.85	16.1	15.35	17	16.69
US-Tk1; PV1	10.54	9.83	9.71	9.62	8.49	12.91	9.56	8.35
US-Tk1; PV2	1.15	1.15	1.15	1.15	1.15	1.15	1.15	1.15

Table 0.5 Table displaying the Broadening of the retrieved inclusion for Phantom 5 at each wavelength. The average difference between the maximum elongation along the three dimensions of target and reconstruction in mm is given.

Broad.(mm)	635 nm	670 nm	830 nm	915 nm	940 nm	980 nm	1030 nm	1065 nm
Tk0; PV1	12.67	13.33	12.67	13.33	12.67	13.33	14	12.67
US-Tk1; PV1	16	14	14	13.33	11.33	16.67	13.33	10
US-Tk1; PV2	-2	-2	-2	-2	-2	-2	-2	-2

PHANTOM 6: Bulk of μ_a = 0.02 mm^{-1} with Inclusion of μ_a = 0.04 mm^{-1}

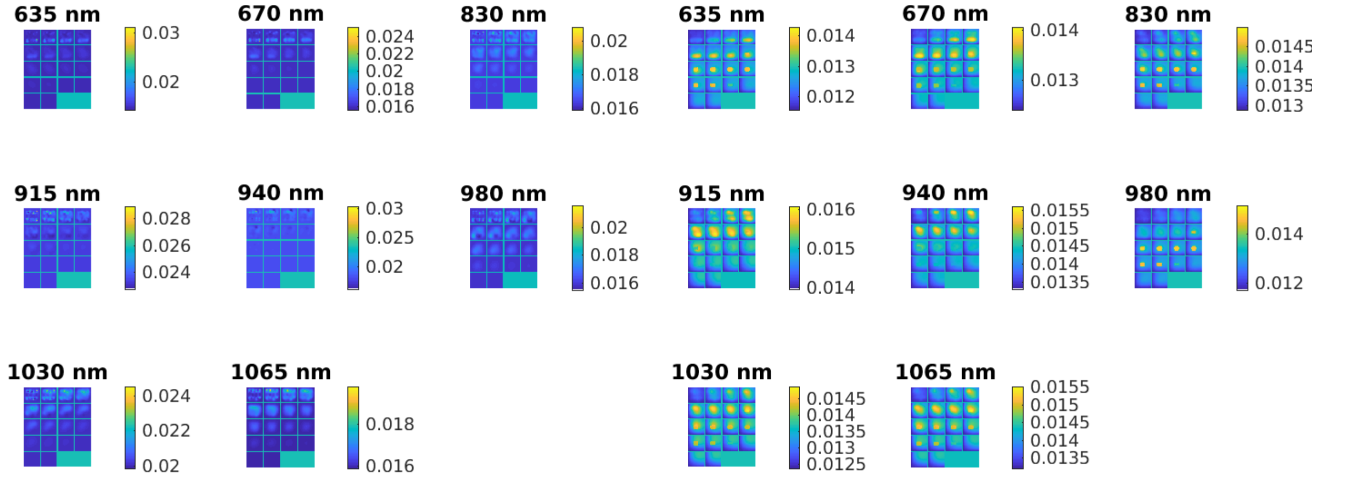

Figure 0.2 Left: Reconstruction of absorption for Phantom 6 when Tk0 regularisation with parameter of 0.2 is applied. Right: Reconstruction of absorption for Phantom 6 when US-Tk1 regularisation with parameter of 1 is applied.

Reconstruction for the phantom with bulk of μ_a = 0.01 mm^{-1} and inclusion of μ_a = 0.04 mm^{-1} is shown in Figure 3.6**Error! Reference source not found.**. As for Phantom 2, the images appear visually noisy for all the wavelengths. The figures of merit are shown from Table 0.6 to Table 0.10. The CNR shows to be lower than the values for Phantom 5, with the same bulk and less absorbing inclusion. The reconstructed contrast shows to be in poor accordance with the target contrast, in line with the case of Tk0. The accuracy error on the absolute absorption value of the inclusion shows an underestimation of ca 60% for all wavelengths. The underestimation in contrast and absolute value is also due to the large regularisation parameter of 1, necessary for better quality images.

Table 0.6 Table displaying the target and reconstructed contrast for Phantom 6 at each wavelength.

C	635 nm	670 nm	830 nm	915 nm	940 nm	980 nm	1030 nm	1065 nm
Target	1.35	1.43	1.49	1.19	1.49	1.46	1.33	1.41
Tk0; PV1	0.12	0.08	0.05	0.04	0.06	0.06	0.05	0.06
US-Tk1; PV1	0.09	0.01	0.06	0.01	0.05	0.12	0.09	0.06
US-Tk1; PV2	0.11	0.04	0.08	0.02	0.03	0.14	0.07	0.06

Table 0.7 Table displaying the Contrast-to-Noise Ratio for Phantom 6 at each wavelength.

CNR	635 nm	670 nm	830 nm	915 nm	940 nm	980 nm	1030 nm	1065 nm
Tk0; PV1	8.6	8.78	6.23	8.7	9.5	4.96	6.79	5.97
US-Tk1; PV1	2.9	0.56	2.8	0.24	1.89	3.42	2.37	1.92
US-Tk1; PV2	2.87	1.66	3.02	0.6	0.85	4.01	1.73	1.77

Table 0.8 Table displaying the Accuracy Error for Phantom 6 at each wavelength.

Acc.	635 nm	670 nm	830 nm	915 nm	940 nm	980 nm	1030 nm	1065 nm
Tk0; PV1	-0.6	-0.57	-0.55	-0.42	-0.48	-0.54	-0.45	-0.54
US-Tk1; PV1	-0.68	-0.67	-0.62	-0.65	-0.6	-0.62	-0.63	-0.59
US-Tk1; PV2	-0.67	-0.66	-0.62	-0.64	-0.61	-0.61	-0.63	-0.59

Table 0.9 Table displaying the Displacement of the retrieved inclusion for Phantom 6 at each wavelength. The Euclidean distance between the centre of the target and reconstruction in mm is given.

Displ.(mm)	635 nm	670 nm	830 nm	915 nm	940 nm	980 nm	1030 nm	1065 nm
Tk0; PV1	19.17	17.47	13.7	17.46	18.71	12.46	15.79	14.54
US-Tk1; PV1	10.34	13.12	6.4	12.9	10.89	3.81	8.87	7.47
US-Tk1; PV2	1.15	1.15	1.15	1.15	1.15	1.15	1.15	1.15

Table 0.10 Table displaying the Broadening of the retrieved inclusion for Phantom 6 at each wavelength. The average difference between the maximum elongation along the three dimensions of target and reconstruction in mm is given.

Broad.(mm)	635 nm	670 nm	830 nm	915 nm	940 nm	980 nm	1030 nm	1065 nm
Tk0; PV1	8	10	16.67	13.33	15.33	14.67	16	17.33
US-Tk1; PV1	22	32	11.33	32	22.67	10.67	8	14
US-Tk1; PV2	-2	-2	-2	-2	-2	-2	-2	-2

4. Conclusion

An assessment of the use of US priors has been presented. The procedure has been tested on multimodal phantoms with the SOLUS probe. For 4 phantoms out of 6 the reconstructions show better quantification of the figures of merit when reconstructing with the *a priori* information. This is particularly true when PV2 is applied. For these phantoms the optimal regularisation parameter is estimated to be between 0.2 and 0.5. Benefits are observed not only for displacement and broadening of the inclusion, but also for all the other figures of merit. Contrast is generally underestimated, however it has correct sign and it is enhanced using US priors. The same underestimation is usually observed also for the absolute values of absorption inside the inclusion. The best results are associated with a CNR greater than 2.5. Further assessments will need to be undertaken to investigate the quality of the data coming from phantom 2 and 6, which will be in the scope of the final deliverable of WP4 (D4.8).

Linking these results to the clinical aim of SOLUS we can conclude that the adoption of US priors in DOT is extremely beneficial. DOT suffers from poor spatial resolution and ill-posedness, which in turn requires strong regularization. Yet, this yields errors in the estimate of the lesion optical properties. As observed above, the use of the US prior improves the quantification of the absorption properties of the perturbation, paving the way to a better estimation of the lesion composition.

Overall, the whole procedure for data analysis is defined, and corresponds to the US-Tk1 regularization with the PV2 norm scheme. The tomographic procedure is streamlined and automated, granting smooth processing of future phantom and in vivo data. The code is flexible enough to include any further possible improvements derived either from the analysis of the final performance assessment of the SOLUS prototype or from the clinical study.